The Film Boiling Reactor: A New Environment for Chemical Processing

Bryan J. Urban and C. Thomas Avedisian
Sibley School of Mechanical and Aerospace Engineering, Cornell University, Ithaca, NY 14853

Wing Tsang
Physical and Chemical Properties Division, National Institute of Standards and Technology, Gaithersburg, MD 20899

DOI 10.1002/aic.10839
Published online May 9, 2006 in Wiley InterScience (www.interscience.wiley.com).

A new platform, based on film boiling, is described for chemical processing by catalytic decomposition of organic liquids. A model for conversion of pure methanol to hydrogen and carbon monoxide is used to illustrate the operational and performance characteristics of the reactor. The model extends film boiling theory to include catalytic reactions at the surface. The results show that wall temperature exerts a dominant influence on product yields, with tube diameter a secondary effect. The yields of hydrogen increase as tube diameter and wall temperature increase, with the variation being nonlinear. At temperatures > 1200 K, the wall conversion rates reach an asymptote with wall concentrations of hydrogen and carbon monoxide being lower and higher than stoichiometric, respectively, because of the higher diffusion rate of hydrogen compared to carbon monoxide. A dimensional "performance factor," defined as the ratio of hydrogen yield to the total energy required to maintain the vapor film and drive the reaction, is used to cast the performance of the film boiling reactor in terms of the variables of the problem. For the range of tube diameters examined (1.5 mm to 1.5 cm), the analysis shows the existence of wall temperatures that optimize performance. The advantages of the new reactor system are its simplicity and potentially large product yields, making it ideal for portable applications.
 AIChE J, 52: 2582–2595, 2006
Keywords: film boiling, hydrogen production, nucleation, chemical reaction, conversion, catalysis, heat transfer, mass transfer, transport, fuel cells

Introduction

Film boiling is usually associated with nuclear meltdown. Less appreciated is that chemical reaction can occur in the film boiling regime and be exploited for useful purposes in chemical processing. Early experimental studies motivated by reactor accident scenarios noted the potential for chemical reaction to occur in the film boiling regime (such as for molten metal/water interactions) but the understanding that emerged from these efforts was limited and of only a phenomenological nature.[1-5] Epstein et al.[6] provided the first rigorous analysis of film boiling on a reactive, noncatalytic surface for stagnation point flow on a flat plate, again in the context of molten metal/water interactions (such as zirconium/water). They noted the potential for producing hydrogen from the zirconium/water reaction at high temperatures (about 1300 K). The operational limits for promoting reactions were not examined. The configuration of molten metal/water interactions as an industrial process for hydrogen production is impractical because of the high temperatures required for the reaction and the liquid containment issues associated with it.

Various authors have reported related film boiling models that do not include chemical reaction:

Current address of B. J. Urban: Department of Mechanical Engineering, Massachusetts Institute of Technology, Cambridge, MA 02139.
Correspondence concerning this article should be addressed to C. T. Avedisian at cta2@cornell.edu.

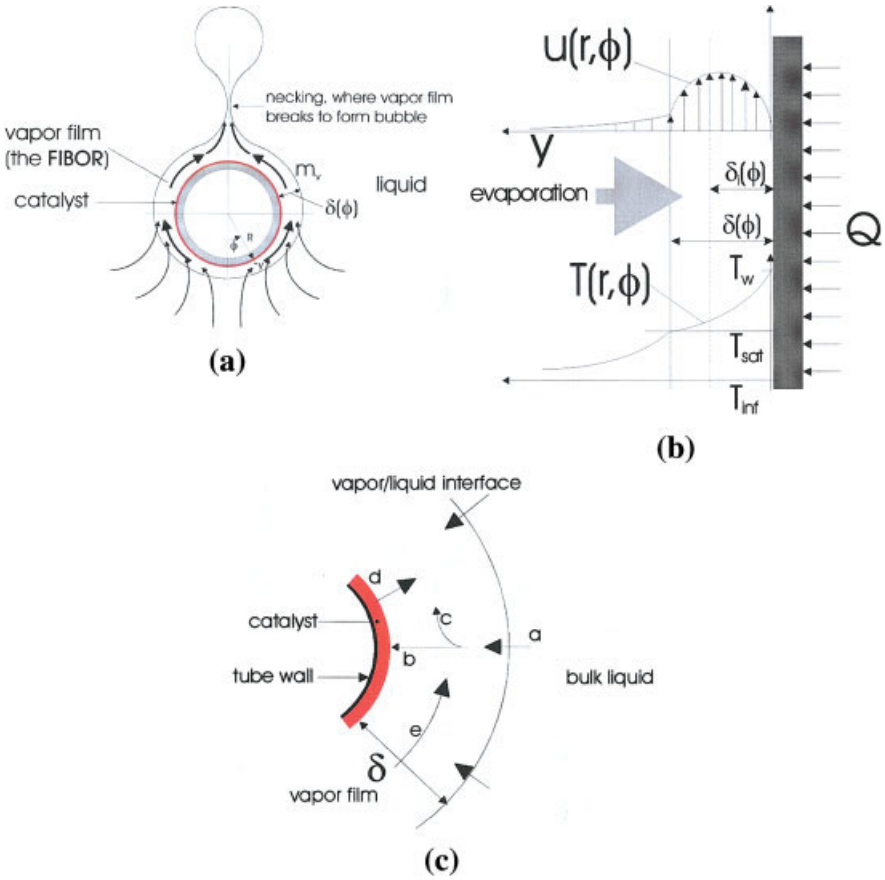

Figure 1. (a) Schematic (idealized) of film boiling configuration for a horizontal tube (not to scale). (b) Schematic of temperature, velocity, and concentration profiles (not to scale). (c) Schematic of transport flow paths during film boiling (not to scale).

[Color figure for parts (a) and (c) can be viewed in the online issue, which is available at www.interscience.wiley.com.]

- *For a vertical plate*: Koh[7]
- *For a horizontal tube*: Sakurai et al.[8] and Sarma et al.,[9] who analyzed the importance of radiation and transport in the liquid and turbulent flow in the film, respectively.
- *Film boiling of miscible liquid mixtures*: Liu et al.,[10] whose model obtained a numerical solution of the governing equations that included mixture transport in the liquid to predict heat transfer coefficients and the influence of boundary conditions (such as radiation and liquid motion).
- *Catalytic decomposition by film boiling of a single-component liquid on a catalyst-coated tube*: Okuyama and Iida,[11] who were the first to measure heat transfer coefficients and noted that hydrogen could be formed by the reaction of methanol. No attempt was made to determine conditions to optimize product yields or to determine the operational parameters that influence it.

The aforementioned investigations suggest the possibilities for effecting chemical change by film boiling. In the following we attempt to establish these observations on a more quantitative basis and describe the system in terms of its potential as a chemical reactor. The emphasis is on the more traditional parameters, such as the influence of process variables and the identification of operating conditions, to optimize product formation associated with chemical reactors. Methanol decomposition was used as a test case because the conditions[11] for conversion are not that much different from those of many other catalytic decompositions. Furthermore, the physical aspects to the system—fluid dynamics and heat transfer—are completely understood. The present analysis is therefore generalizable to other catalytic systems. An important aim of this paper is to call attention to the technical community with respect to the potentialities of this system.

We choose a horizontal tube to analyze and focus on hydrogen yield and use rate constants pertinent to a platinum-black catalyst in methanol.[11] The horizontal tube configuration is simple and the concept can be envisioned for scale-up in industrial applications. Including hydrogen in the performance metric is in keeping with interest in alternative methods for producing hydrogen from organic liquids as a fuel for power and propulsion. Indeed, one of the most impressive aspects of the system described is its simplicity compared to that of traditional chemical reactor systems. This may be particularly important for practical systems for generating hydrogen.

Figure 1a schematically illustrates a cross-sectional view of the film boiling configuration for a horizontal tube in a stagnant liquid pool. Shown are the tube, vapor film, and transport paths around the cylinder that lead to pinching of the vapor ligament and formation of a free bubble. Figure 1b shows additional details of the flow and concentration boundary layers and temperature distribution across the film. Figure 1c illustrates

the paths envisioned for transport and reaction of chemical species in the film for surface reaction promoted by a catalyst coating the tube surface. As illustrated in Figure 1c, organic liquid evaporates (a) and diffuses to the surface (b). Part of the reactant is carried around the tube (c) in the vapor film (thickness δ) arising from flow (e) and part makes it to the wall (b), where it is adsorbed and reacts. Products diffuse back into the film (d) where they are carried around the tube surface and expelled through the percolating bubbles. In most instances we can expect that the composition of the bubble will contain both reactants and products. We term the process of chemical reaction by the method as described above a *film boiling reactor* (or FIBOR).

Catalytic reaction in a FIBOR has the potential for high-temperature thermal decomposition, steam reforming, and water–gas shift reactions in a cold bulk liquid containment. It avoids some of the high-temperature containment requirements of other reactor designs such as packed bed reactors. A FIBOR accomplishes this by a natural separation of the high-temperature reacting (vapor) volume from the cooler bulk liquid. In this respect, the reactor itself—the vapor volume bounded on one side by a catalytic surface—could be considered as self-assembled as it forms as a natural consequence of heat transfer from a heated horizontal tube in a relatively cold bulk liquid through the phase change/boiling process.

The vapor/catalyst combination analyzed in this study is methanol/platinum black, and the vapor bubbles will essentially contain methanol, CO, and H_2 where the latter two species are reasonably insoluble in methanol. The problem is to predict the film thickness and product yields, which is equivalent to the flow rates of species around the tube surface, and how variables (surface temperature and tube diameter) influence them. The goal with such an analysis is to determine the efficacy of film boiling as a potentially useful configuration in which to do reaction engineering. The emphasis is on aspects occurring within the vapor film that govern operation of a FIBOR by using a model that captures the elements of the problem and that allows one to understand the influence of operational parameters on performance. The related problems of analyzing how bubbles form in film boiling with reaction, then detach from the tube and carry with them the reaction products, and the operations required to separate the chemical species inside the bubbles after the bubbles break through the free liquid surface of the reactant pool and release the product gases, are outside the scope of this study.

The article is organized as follows. We discuss the chemistry of methanol decomposition and then outline the transport model that couples heat and mass diffusion with chemical reaction. The liquid/catalyst combination analyzed in this study is methanol/platinum black because of the availability of rate constant expressions for this combination.[11] The task is to predict the film thickness and product yields and how surface temperature and tube diameter influence them. Mass transfer is included by an integral method that uses a third-order variation with distance across the vapor film and with the constants satisfying the boundary conditions. Results are presented that illustrate the influence of parameters on product yield. Although the calculations are based on methanol decomposition, the results can be extended to other reaction chemistries for which a suitable catalyst and rate constant are available.

Chemistry

The transformation of methanol gas into a hydrogen-rich mixture is a multistep process that involves a variety of mechanisms,[12] depending on the catalyst. For example, the intermediate reactions are

$$CH_3OH \rightarrow HCHO + H_2 \tag{1}$$

$$HCHO \rightarrow CO + H_2 \tag{2}$$

For simplicity we express the overall conversion of methanol by the global reaction

$$CH_3OH \xrightarrow{K} CO + 2H_2 \tag{3}$$

where K is the overall rate constant for the catalyst. By the stoichiometry of Eq. 3, for every 2 moles of hydrogen the system produces 1 mole of carbon monoxide. The global reaction will capture the essential features of the coupling between chemical reaction and heat/mass transfer that is at the heart of the FIBOR. Without a catalyst methanol will not decompose to produce hydrogen at the operational temperatures of interest for a FIBOR.

In treating the conversion process by the single-step reaction, details of the complex kinetic behavior associated with intermediate reaction steps and the process of adsorption and conversion at the molecular level are lumped into the rate expression and are thus not explicitly considered. We assume that the characteristic time of catalysis is much smaller than that of desorption (as is the case for this reaction) so that nearly all active sites will be covered by strongly adsorbed species.[12,13] Considering a rate-controlled process is more complex and outside the scope of the analysis.

In the present study, each species reacts at a surface rate given by

$$w_i = \varpi_i Y_{CH_3OH,w} \tag{4a}$$

where

$$\varpi_i = \frac{\nu_i W_i \bar{W}}{W_{CH_3OH}} PK \tag{4b}$$

and the rate constant K is

$$K = A \exp\left(-\frac{E}{R_o T_w}\right) \tag{4c}$$

In Eq. 4a, w_i is the mass flux of species i produced or consumed by chemical reaction (kg m^{-2} s^{-1}), the W values are molecular weights, the ν values are stoichiometric coefficients (that is, $\nu_{CH_3OH} = 1$, $\nu_{CO} = 1$, $\nu_{H_2} = 2$), and we have taken $\bar{W}$ as the mean molecular weight. We should note that the predicted trends are not strongly influenced by more rigorous definitions of $\bar{W}$. By choosing a single value for $\bar{W}$, independent of species

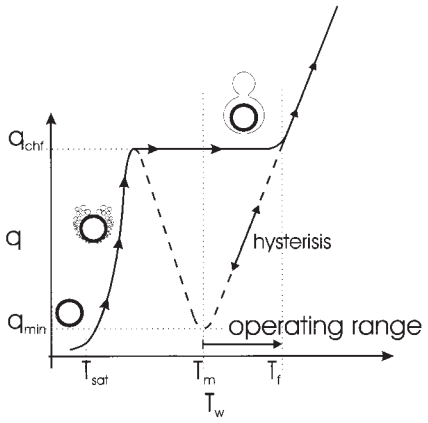

Figure 2. Operational range of a FIBOR.

mass fraction, there is then only one unknown variable to consider: the mass fraction of methanol at the wall, $Y_{CH_3OH,w}$. In what follows we take $\bar{W}$ as an intermediate value between 100 and 0% yield (that is, $11 \leq \bar{W} \leq 32$, for a gas mixture consisting of CO + $2H_2$ or methanol). We found that the influence of parameters is not changed by selecting a mean molecular weight in this range.

The values for E and A we use are those determined by Okuyama and Iida[10] from experiments on catalytic conversion of methanol in a packed bed reactor using a platinum black catalyst and then corrected based on measured heat transfer coefficients of a catalyst-coated tube in film boiling in methanol:

$$E = 6.82 \times 10^4 \qquad \text{(J/mol)} \tag{5a}$$

and

$$A = 17.54 \times 10^4 \qquad [\text{mol}/(\text{m}^2\,\text{s}^{-1}\,\text{MPa}^{-1})] \tag{5b}$$

As expected, the results are very sensitive to the activation energy because this parameter appears in an exponential in Eq. 4c, tied with these values. Because they are derived from measurement,[11] using them provides an ability to illustrate the influence of parameters on a more realistic performance of the FIBOR concept than would otherwise be possible with arbitrary values of A and E.

Operational Limits

The operational limits of a FIBOR are governed by the boiling curve for a fluid, a general schematic of which is shown in Figure 2.[14] To establish a vapor film, it is necessary that $T_w > T_m$. Various models[15-19] for T_m result in values in the range of 400 to 500 K for methanol, independent of the transport situation for the fluid (such as models that assume T_m is the same as the limit of superheat of a fluid).

Under the action of a constant heat flux boundary, the critical heat flux (CHF, q_{chf}) has to be reached to establish the vapor film whereby T_w jumps to T_f as indicated in Figure 2. Formulations for predicting CHF for horizontal tubes are well established.[14] The absolute upper limit on T_w is the melting point of the tube metal, such as 1800 K for stainless steel. Under some conditions, it is possible that T_f is greater than the melting point, in which case the experimental configuration is physically destroyed upon reaching q_{chf}. In practice, one obviously wishes to avoid this situation with proper design of a FIBOR.

Once the vapor film is established a power reduction below the critical heat flux lowers T_w toward T_m arising from hysteresis that is typical of film boiling. Further reduction of the heat flux beyond $q_{\min}$ destabilizes the film and reestablishes nucleate boiling. The practical operating limit of a FIBOR is between T_m and a temperature that is less than the softening point of the metal. To avoid this situation, establishing a FIBOR may require an automated power reduction capability to sense wall temperature and/or its time rate of change.

Analysis

We use an integral mass balance approach in the concentration boundary layers, coupled with a solution to the momentum and energy equations for transport in the vapor film for a simplified set of assumptions, to model reaction, product development, and transport through the vapor film. The major assumptions around which the analysis is based are the following:

(1) Reactant liquid is at saturation conditions
(2) Radiation is negligible
(3) Boundary condition at the liquid/vapor interface is intermediate between zero shear and zero slip
(4) $\delta/\chi \ll 1$, where χ is the arc length along the tube surface
(5) Only surface reactions occur on the catalyst-coated tube
(6) Laminar flow in the vapor film and the liquid/vapor interface is stable
(7) Catalyst does not degrade and coke does not form during operation
(8) Bulk liquid is stagnant

The above assumptions create a useful starting point to analyze operation of a FIBOR. While the formation of coke limits performance, the Fibor concept is versatile enough to incorporate modifications that address this problem.

The importance of radiation has been shown to depend on the extent of subcooling of the bulk liquid and emissivity of the tube. For film boiling from horizontal tubes in saturated liquids the radiation contribution is generally small.[8,10]

The vapor film in film boiling depicted in Figure 1 is characterized by a smooth interface. Otherwise, the film can exhibit a wavy character, especially for large tube diameters. Accounting for the generation of an unstable wave pattern, and the detachment and percolation of bubbles through the liquid pool is beyond the scope of this study. Film boiling with a smooth liquid/vapor interface will occur when $R/\lambda_{crit} \leq 0.63$[14,20] and $\text{Re}_\delta < 100$,[21] where λ_{crit} is the Taylor unstable wavelength for bubble detachment from the surface. These conditions are satisfied by choice of parameters in the present study. At larger tube diameters, an unstable wave pattern exists at the liquid/vapor interface, which results in a wavy pseudoturbulent flow pattern of bubbles around the periphery of the interface, and within the vapor film.[21]

A scale analysis on the momentum equation written in cylindrical coordinates shows that if $\text{Re}_\delta(\delta/\chi)^2 \ll 1$, where $\text{Re}_\delta = u_{rep}\delta/\nu$, u_{rep} is a representative velocity in the ϕ direction in the film, and χ is the arc length along the tube surface (that is,

$\chi = R\phi$), then inertia can be neglected and friction is balanced by gravity to give

$$g(\rho_l - \rho_v)\sin\phi + \mu_v \frac{\partial^2 u}{\partial y^2} = 0 \tag{6}$$

where $y = r - R$ and the solution domain is $0 \le y \le \delta$. The simplification of Eq. 6 is based on the product of Re_δ and $(\delta/\chi)^2$ being small. For the conditions of this study, Re_δ is of order 10 as will be seen later when the model results are discussed. The neglect of inertia then rests on $\delta/\chi \ll 1$, which breaks down at the stagnation point of the cylinder and as $\phi \to 180°$, where we will see that δ exhibits a singularity.

Similarly, scale analysis on the energy equation shows that energy transport in the vapor film is largely one of conduction across the film if $Pr\ Re_\delta(\delta/\chi)^2 \ll 1$, where Pr is the Prandtl number of the vapor and, again, it is the product of these variables (and not on the individual terms) being much less than unity that makes this assumption valid. With $Re_\delta(\delta/\chi)^2 Pr \ll 1$ the energy equation then simplifies to

$$\frac{\partial^2 T}{\partial y^2} = 0 \tag{7}$$

Diffusion of reactants and products in the vapor film is analyzed by a global method as discussed in the following text.

The boundary conditions for fluid, thermal, and mass transport are taken to be the following:

$$y = 0\text{: } T = T_w \qquad u = 0 \qquad Y = Y_{iw}$$
$$\frac{\partial Y_i}{\partial y} = -\frac{\varpi_i}{\rho_v D_{i,m}} Y_{CH_3OH,w} \qquad \frac{\partial^2 Y_i}{\partial y^2} = 0 \tag{8a}$$

$$y = \delta\text{: } T = T_s \qquad \mu_v \frac{\partial u}{\partial y} = \mu_l \frac{\partial u_l}{\partial y} \qquad \frac{\partial Y_i}{\partial y} = 0 \tag{8b}$$

where w_i is the rate of formation of species i by chemical reaction at the surface (Eqs. 4 and 5). A discussion of the species mass fraction boundary conditions at $y = 0$ and $y = \delta$ is given in Appendix A.

Based on Eq. 8b, transport in the liquid should in general be considered. However, doing so considerably complicates the analysis. As written, Eq. 8b states that the shear is matched at the liquid/vapor interface and, thus, that liquid motion must be considered in the analysis. There is a historical basis in film boiling analysis for treating the liquid as completely stagnant, beginning with the first study of Bromley[22] for film boiling without chemical reaction. Later work by Koh[7] included fluid motion in the bulk liquid for film boiling on a vertical plate in a saturated liquid without chemical reaction in the vapor film. Results showed that the magnitude of the liquid velocity induced by flow in the film was quite small compared to the maximum vapor velocity in the film. More recent analyses have compared results when motion is included to neglecting it completely[8,9]—for cases where there is no surface reaction—which have shown comparatively small differences. The inclusion of transport in the liquid and radiation in the vapor is a problem for future work when considering subcooled liquids. Further discussion of boundary conditions is given in Appendix A.

The influence of liquid motion on vapor transport comes through the boundary condition at the liquid/vapor interface. Lienhard[14] notes that the surrounding liquid is not easily set into motion by the shear stress at the liquid/vapor interface. This consideration is the basis for a boundary condition at the liquid/vapor interface $y = \delta$ that is intermediate between a zero stress and no slip condition:

$$u = 0 \qquad \text{or} \qquad \frac{\partial u}{\partial y} = 0 \tag{9}$$

The important point is that invoking either of Eqs. 8 removes from consideration transport in the liquid. This simplifies what is already a complex problem. Nonetheless, the basic features of reaction in the vapor film are still captured. We later show that some of the important aspects of the problem such as optimal operational conditions (for tube diameter and temperature) have a comparatively weak dependency on the type of boundary condition assumed at $y = \delta$, whether no slip or zero shear.

An integral energy balance on a control volume that is bounded by ϕ and $\phi + \Delta\phi$, and δ and $\delta + \Delta\delta$ (see Figure B1 in Appendix B) equates the enthalpy carried by the vapor flowing around the cylinder in the film to enthalpy transported across the liquid/vapor interface by evaporation of methanol and heat conducted into the vapor film at the surface of the cylinder. A mass balance on the control volume eliminates the mass flux across the liquid/vapor interface to give (see Appendix B)

$$\rho_v \int_0^\delta u[L + c_{pv}(T - T_{sat})]dy = -k_v \frac{d}{2}\int_0^\phi \left.\frac{\partial T}{\partial y}\right|_{y=0} d\phi \tag{10}$$

Equation 10 provides the condition to determine how δ varies with parameters.

The velocity u in Eq. 10 is the mass-weighted average velocity in the ϕ direction. The solution of Eqs. 6 and 7 with Eqs. 8a and 9 gives u as

$$u = \frac{g(\rho_l - \rho_v)}{2\mu_v} \sin\phi(m\delta y - y^2) \tag{11}$$

where $m = 1$ is the no slip condition and $m = 2$ is the zero shear stress condition. The temperature distribution across the vapor film is linear from Eq. 7, so that

$$T = T_w - \Delta T_{sat}\frac{y}{\delta} \tag{12}$$

Substituting Eqs. 11 and 12 into Eq. 10 and solving for the vapor film thickness δ gives

$$\delta = \sqrt{2}\, B^{1/4} \frac{(\int_0^\phi \sin^{1/3}\phi d\phi)^{1/4}}{\sin^{1/3}\phi} \tag{13}$$

where

$$B = \frac{\frac{4}{6m-4}\, c_{pv}\cdot \Delta T_{sat}}{L\left\{1+\frac{2m-1}{6m-4}\frac{c_{pv}\cdot \Delta T_{sat}}{L}\right\}} \frac{\frac{k_v}{c_{pv}\rho_v}\frac{\mu_v}{\rho_v}}{g\left(\frac{\rho_l\rho_v}{\rho_v}\right)} d \tag{14}$$

Within the region $0 \le y \le \delta$, we assumed that the concentration boundary layers reached the liquid/vapor interface (that is, $\delta_i \approx \delta$ in Figure 1b). This assumption considerably simplifies the analysis, and we later verified that it is a reasonable assumption for the variable ranges of interest to our process. We approximate the concentrations of product species by third-order polynomials that satisfy the boundary conditions of Eqs. 8a and 8b:

$$Y_{H_2} = Y_{H_2,w} - \frac{\varpi_{H_2} Y_{CH_3OH,w}}{\rho_v D_{H_2,m}} y + \frac{\varpi_{H_2} Y_{CH_3OH,w}}{3\rho_v D_{H_2,m}\delta^2} y^3 \tag{15}$$

$$Y_{CO} = Y_{CO,w} - \frac{\varpi_{CO} Y_{CH_3OH,w}}{\rho_v D_{CO,m}} y + \frac{\varpi_{CO} Y_{CH_3OH,w}}{3\rho_v D_{CO,m}\delta^2} y^3 \tag{16}$$

We feel that a third-order polynomial assumption is a reasonable one to capture the reaction and diffusion process in the vapor film to illustrate capabilities of a FIBOR. It was also used by Okuyama and Iida[11] to analyze their measurements of film boiling. As noted previously, the rate constant parameters (Eq. 5) were obtained by fitting them with measured heat transfer coefficients in a model similar to the one discussed here. In this manner, the assumption of a third-order variation of mass fraction with these parameters is acceptable. Because the mass fraction of components must sum to unity everywhere in the film,

$$Y_{CH_3OH} + Y_{CO} + Y_{H_2} = 1 \tag{17}$$

we can write for Y_{CH_3OH} that

$$Y_{CH_3OH} = Y_{CH_3OH,w}\left[1 + \frac{1}{\rho_v}\left(\frac{\varpi_{H_2}}{D_{H_2,m}} + \frac{\varpi_{CO}}{D_{CO,m}}\right) y - \frac{1}{3\rho_v\delta^2}\left(\frac{\varpi_{H_2}}{D_{H_2,m}} + \frac{\varpi_{CO}}{D_{CO,m}}\right) y^3\right] \tag{18}$$

The importance of knowing the wall concentration of methanol is that it determines the mass throughput of species through the vapor film as a function of the angle ϕ. For methanol, the mass throughput is expressed as

$$M^*_{0-\phi,CH_3OH} = \rho_v \int_0^\delta u(1 - Y_{CH_3OH})dy = (\varpi_{H_2} + \varpi_{CO})\frac{d}{2}\int_0^\phi Y_{CH_3OH,w} d\phi \tag{19}$$

For hydrogen and carbon monoxide,

$$M^*_{0-\phi,H_2} = \rho_v \int_0^\delta u Y_{H_2} dy = M^*_{0-\phi,CH_3OH}\frac{\varpi_{H_2}}{(\varpi_{H_2} + \varpi_{CO})} \tag{20}$$

and

$$M^*_{0-\phi,CO} = \rho_v \int_0^\delta u Y_{CO} dy = M^*_{0-\phi,CH_3OH}\frac{\varpi_{CO}}{(\varpi_{H_2} + \varpi_{CO})} \tag{21}$$

The total gas throughput in the vapor film around the cylinder (that is, from $\phi = 0°$ to $\phi = 180°$) is

$$M^*_{total} = 2\rho_v \int_0^\delta u dy_{\phi=180} \approx 2.040(2^{5/2}B^{3/4})\rho_v\left(\frac{3m-2}{6}\right)\frac{g(\rho_l - \rho_v)}{2\mu_v} \tag{22}$$

where the right-hand side of Eq. 22 is obtained with the aid of Eq. 11.

The total molar throughput N_i (mol h^{-1} m^{-1}) is found by dividing the mass throughput $M^*_{0-\phi,i}$ with $\phi = 180°$ from Eqs. 19–21 by the molecular weight W_i:

$$N_i = \frac{M^*_{0-180,i}}{W_i} \tag{23}$$

The reaction proceeds stoichiometrically according to Eq. 1 so that the molar throughput of CO will be half that of H_2 and the mass throughput of CO will be sevenfold that of H_2 (that is, $W_{H_2} = 2$ and $W_{CO} = 28$). For later reference, the mole fraction n_i of individual components is related to mass fractions Y_i as

$$n_i = \frac{Y_i/W_i}{\sum_{\text{all species}} Y_i/W_i} \tag{24a}$$

$$\sum_{\text{all species}} n_i = 1 \tag{24b}$$

To determine the mass fraction of methanol at the wall, Eq. 11 is substituted into Eq. 19 and differentiated with respect to ϕ to give

$$\frac{d}{d\phi}\left[\sin\phi(C_1\delta^4 Y_{CH_3OH,w} + C_2\delta^3 - C_2\delta^3 Y_{CH_3OH,w})\right] = C_3 Y_{CH_3OH,w} \tag{25}$$

where

$$C_1 = (48m - 35)\left(\frac{\varpi_{CO}}{D_{CO,m}} + \frac{\varpi_{H_2}}{D_{H_2,m}}\right) \tag{26}$$

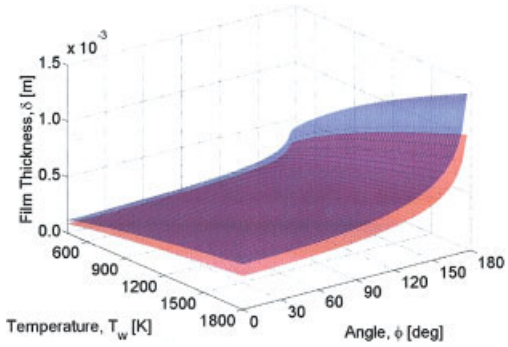

Figure 3. Vapor film thickness vs. angle (see Figure 1) and wall temperature for $m = 1$ (blue) and $m = 2$ (red).

[Color figure can be viewed in the online issue, which is available at www.interscience.wiley.com.]

$$C_2 = 30\rho_v(3m - 2) \tag{27}$$

and

$$C_3 = \frac{-360\mu_v}{g(\rho_l - \rho_v)}(\varpi_{H_2} + \varpi_{CO})\frac{d}{2} \tag{28}$$

Expanding Eq. 25 yields

$$C_3 Y_{CH_3OH,w} = \cos\phi[C_1\delta^4 Y_{CH_3OH,w} + C_2\delta^3(1 - Y_{CH_3OH,w})] + \sin\phi\left\{C_1\left(4\delta^3\frac{d\delta}{d\phi}Y_{CH_3OH,w} + \delta^4\frac{dY_{CH_3OH,w}}{d\phi}\right) + C_2\left[3\delta^2\frac{d\delta}{d\phi}(1 - Y_{CH_3OH,w}) - \delta^3\frac{dY_{CH_3OH,w}}{d\phi}\right]\right\} \tag{29}$$

which, with Eq. 13 for δ, is the equation for methanol concentration at the wall. A condition for $Y_{CH_3OH,w}$ to integrate Eq. 29 at $\phi = 0$ also comes from Eq. 29 evaluated at $\phi = 0°$:

$$Y_{CH_3OH,w}|_{\phi=0} = \frac{C_2\delta^3}{C_1\delta^4 + C_2\delta^3 - C_3} \tag{30}$$

The various integrals that appear in the above set of equations were computed using a Lobatto quadrature method from the MATLAB library. The function attempts to approximate the integral over an interval with an error tolerance of 10^{-9} using a high-order recursive adaptive quadrature. The accuracy of the integration was tested against several functions with known integrals to ensure reliability and accuracy.

In cases where the Lobatto quadrature was used as an intermediate step, the technique was applied many times. To compute δ as a function of ϕ, the function was integrated on 1000 subintervals from $\phi = 0°$ to $\phi = 180°$. In this way, δ is known for 1000 evenly spaced points from 0 to 180°. Equation 29, integrated using a fourth-order Runge–Kutta formulation, requires evaluation of inner and outer integrals. Quadrature was used on the inner function and Simpson's rule was applied to the outer function.

The mass fraction of methanol at the wall was obtained for 1000 equally spaced intervals from $\phi = 0°$ to $\phi = 180°$ by numerical integration of Eq. 29 using Eq. 30 as the initial condition. Methanol throughput was then computed at each step in ϕ from Eq. 19, and the result used to find the CO and H_2 throughputs from Eqs. 20 and 21, respectively. The values of $Y_{CO,w}$ and $Y_{H_2,w}$ were obtained from Eqs. 20 and 21 and compared with Eq. 17 as a consistency check.

The question of verification of the model and assumptions is addressed through the selection of the particular rate parameters of Eq. 5. As noted previously, these values were determined[11] by fitting experimentally measured heat transfer coefficients for horizontal tubes in film boiling with predicted values from a model that assumes a stagnant liquid with a third-order polynomial approximation for the species mass fractions by using the rate values as fitting parameters. As a result, predicted trends using these rate parameters should provide a reasonable expectation of how a FIBOR would perform. Recognizing that the rate parameters exert a strong influence on quantitative predictions, we prefer to use a model that is paired with a specific set of rate parameters. As such, we expect that the predicted trends should be reasonable for how parameters will influence product yields, and illustrate the operational limits of the FIBOR, which is our main purpose.

Results

Figure 3 shows the dependence of film thickness on ϕ and T_w for a 5 mm diameter tube. In the following, we take T_w up to 1800K to illustrate how variables influence the results. In practice, of course, the tube melting temperature limits T_w and the FIBOR is destroyed at that point. All properties are evaluated at 0.10 MPa and at an average film temperature $T_{avg} = 0.5(T_{sat} + T_w)$, unless otherwise noted. The exception is thermal conductivity for which we used a value 1.4 times that of methanol (that is, as in Ref. 11). In this figure and all of the results presented, all required physical properties are extracted from accepted literature correlations.[23,24] In Figure 3, predictions using the two boundary conditions of Eq. 9 are shown; differences are within a factor of 2, which reflects the influence of boundary condition at the liquid/vapor interface. At $\phi = 180°$ δ is singular. Using Eq. 11, and from Figure 3, represen-

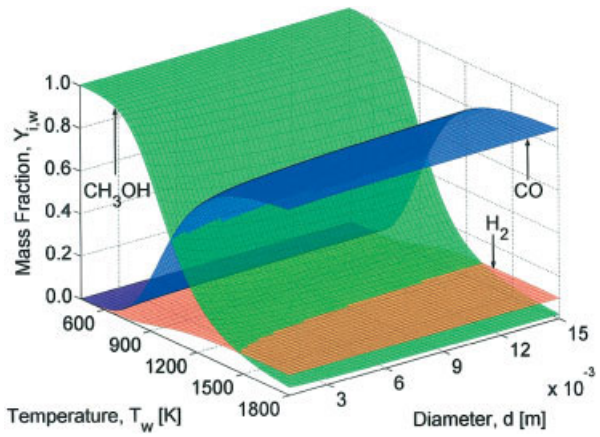

Figure 4. Wall mass fraction as a function of wall temperature and diameter.

[Color figure can be viewed in the online issue, which is available at www.interscience.wiley.com.]

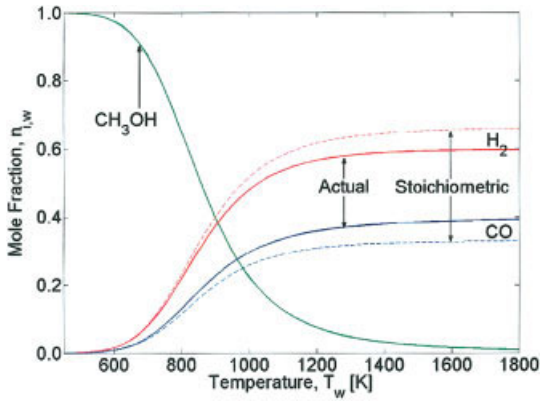

Figure 5. Wall mole fraction vs. wall temperature for a 5-mm wire and $m = 1$.

[Color figure can be viewed in the online issue, which is available at www.interscience.wiley.com.]

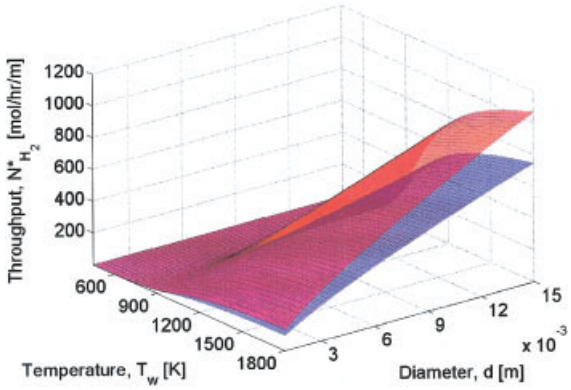

Figure 7. Hydrogen yield (molar throughput) as a function of process variables.

[Color figure can be viewed in the online issue, which is available at www.interscience.wiley.com.]

tative values (at 1000 K) of velocity and film thickness are 5 m/s and 300 μm, respectively (that is, using $\phi \simeq 90°$ as representative), for a cylinder diameter of 5 mm. With $\nu \simeq 9.2 \times 10^{-5}$ m^2/s, $\chi \simeq 0.008$ m, and Pr $\simeq 1$, then $\mathrm{Re}_\delta = u_{rep}\delta/\nu \simeq 16$ and $\delta/\chi \simeq 0.038$. Therefore $\mathrm{Pr}\,\mathrm{Re}_\delta(\delta/\chi)^2 \approx 0.02$, which is consistent with the approximations made.

Figure 4 shows the dependency of wall mass fraction $Y_{i,w}$ on tube temperature and diameter for $m = 1$. At high temperatures, $Y_{\mathrm{CH_3OH},w}$ approaches zero as methanol catalytically decomposes at the wall, whereas the sum of $Y_{\mathrm{H_2},w}$ and $Y_{\mathrm{CO},w}$ approaches unity to satisfy Eq. 17. Increasing the wall temperature in the high-temperature range cannot produce an appreciable change in the mass fractions of products. This fact translates into slowing the rate of change of hydrogen yield with temperature. At high temperatures, where methanol completely decomposes at the wall, one might expect the concentrations to approach the stoichiometric mass fraction ratio of $Y_{\mathrm{CO},w} : Y_{\mathrm{H_2},w}$ of 7:1, or mole fraction ratio, $n_{\mathrm{CO},w} : n_{\mathrm{H_2},w}$, of 1:2. However, given that hydrogen diffuses faster than carbon monoxide because of the higher diffusion coefficient for hydrogen compared to carbon monoxide,[23] the amount of hydrogen at the wall is lower than stoichiometric, and for carbon monoxide it is higher than stoichiometric. The differences increase as temperature increases as a result of enhanced diffusion at high temperatures. To better illustrate this behavior, Figure 5 shows the influence of wall mole fraction, $n_{i,w}$, with surface temperature for one particular tube diameter of 5 mm.

Figure 6 shows how the total mass processed in the vapor film, M^*_{total} (units of kg h^{-1} m^{-1}), varies with wall temperature and tube diameter. The two surfaces in the figure are for boundary conditions corresponding to $m = 1$ and $m = 2$ (Eq. 9). Differences for the two conditions are again within a factor of 2. The results show that the amount of reactant that can be processed is quite large.

Figure 7 shows the dependency of molar throughput in the vapor film, $N_{\mathrm{H_2}}$ and $N_{\mathrm{H_2},0-180}$ from Eqs. 21 and 24, on wall temperature and tube diameter. The hydrogen yield is comparatively high for tube diameters $\gtrsim 9$ mm and for temperatures of >800 K, and are close to hydrogen production in portable generators mentioned in the literature.[25] As noted previously, other organic liquids can be used such as ethanol and aqueous mixtures.

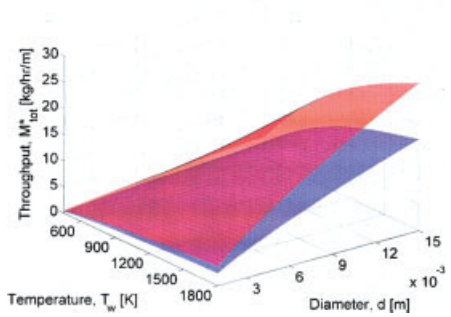

Figure 6. Total mass of methanol processed (includes both reacted and unreacted methanol traveling through the system).

[Color figure can be viewed in the online issue, which is available at www.interscience.wiley.com.]

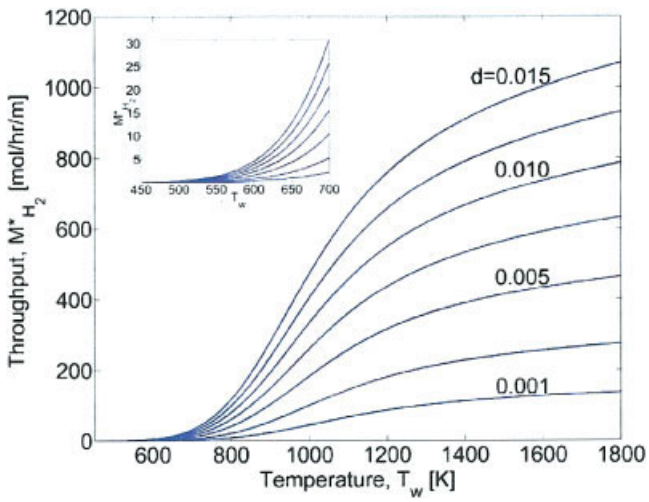

Figure 8. Predicted hydrogen yields ($m = 2$ only shown) for constant tube diameter.

Inset shows low-temperature range. [Color figure can be viewed in the online issue, which is available at www.interscience.wiley.com.]

As the temperature or diameter increases, the vapor velocity increases as well, which increases the hydrogen throughput. With an increase in temperature, the reaction rate (ω_i) also increases, which increases H_2 and CO yields. Figure 8 is a cross-plot of N_{H_2} with T_w and d. At low temperatures (<800 K), the total vapor throughput and the amount of methanol reacting are both comparatively small in this range. At medium temperatures (800–1200 K), the vapor throughput reaches a modest value but, more important, the fraction of reacted methanol increases. In this temperature range, ϖ_i increases rapidly. To satisfy the hydrogen mass balance of Eqs. 17 and 20, ϖ_i increases so that $Y_{CH_3OH,w}$ decreases, whereas $Y_{CO,w}$ and $Y_{H_2,w}$ both increase. This results in a high fraction of H_2 and CO in the vapor film, thus causing a rapid increase in N_{H_2} and N_{CO}.

In chemical systems the time available for chemical reaction, which we term the "residence time," is an important parameter to characterize reactor performance. To give the reader a better feeling about the reaction process, we calculated the influence of parameters on residence time. We take a simple scaling of the residence time as the time for a packet of fluid to be transported around the tube in the vapor film at a representative velocity, u_{rep}:

$$t_{res} = \frac{(\pi d/2)}{u_{rep}} \tag{31}$$

The representative velocity around the tube circumference was determined by first averaging u in Eq. 11 across the film thickness and then from that result computing the average velocity around the circumference, $0° \le \phi \le 180°$:

$$u_{rep} = \frac{2B^{1/2}}{\pi}\left(\frac{3m-2}{6}\right)\frac{g(\rho_l-\rho_v)}{2\mu_v}\int_0^{\phi}\sin^{1/3}\phi\left(\int_0^{\phi}\sin^{1/3}\phi d\phi\right)^{1/2}d\phi \tag{32}$$

Numerically integrating Eq. 32 gives

$$u_{rep} \approx 1.766B^{1/2}\left(\frac{3m-2}{6}\right)\frac{g(\rho_l-\rho_v)}{2\mu_v} \tag{33}$$

Figure 9 shows how the residence time varies with T_w and d for $m = 1$ and $m = 2$. The trends are consistent with the scaling $t_{res} \simeq d^{1/2}[\Delta T_{sat}/(1 + C\Delta T_{sat})]^{1/2}$, which follows from Eqs. 14 and 31, where C depends on fluid properties. As T_w is reduced, the residence time increases and the reaction slows because of the strong dependency of the rate constant on temperature. As the tube diameter increases the residence time increases as well. Figure 9 shows that residence times in the FIBOR are in the range of 1 to 20 ms. This situation resembles conditions encountered in the short contact time reactors described by Deluga et al.[26]

Although there are some similarities of a FIBOR with other reactor configurations (such as packed bed reactors) there are also notable differences. Tubular reactors allow for independent adjustment of operating temperature and reactant flow rate

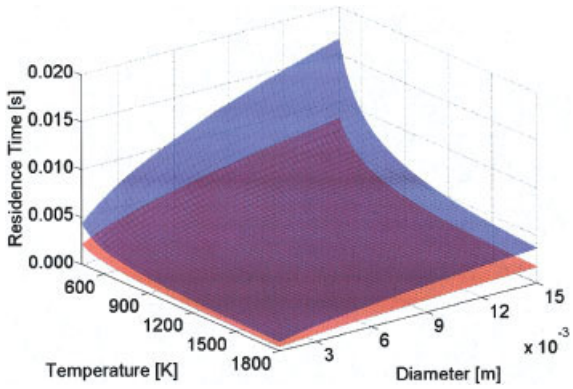

Figure 9. Time available for methanol production in vapor film.

[Color figure can be viewed in the online issue, which is available at www.interscience.wiley.com.]

and thus may be considered to have two degrees of freedom. This is not the case for a FIBOR. For a FIBOR, the flow rate is determined by the wall temperature and physical configuration. Furthermore, the reactor volume itself is determined by evaporation of bulk liquid, which is a function of the wall temperature—a consequence of self-assembly of a FIBOR. Thus, we lose a degree of freedom in operating a FIBOR relative to more conventional reactor systems. This concern is offset by the fact that one does not need high-temperature containment of a FIBOR and the reactant serves as its own insulator.

To better evaluate the operation of a FIBOR, we define a dimensional quantity termed the "performance factor" as the ratio of molar throughput of hydrogen to the total energy required by the system:

$$\varepsilon = \frac{N_{H_2}}{Q_{tot}} \qquad [(\text{mol/h})/(\text{W})] \tag{34}$$

ε is similar to an efficiency in that it is a measure of the amount of hydrogen that can be produced per unit total energy. It does not consider any parameters of the catalytic surface. In particular, the model assumes that the catalytic surface to be infinitely operable with no degradation during operation. A more rigorous definition would have to include the effectiveness of the catalytic surface and such parameters as porosity, chemical activity, and adsorption.

The variation of N_{H_2} with wall temperature and tube diameter has already been displayed in Figure 7. Q_{tot} is the total power needed to maintain the boiling and reaction processes. It is the sum of the power required for film boiling (heat conduction through the vapor film + heat of vaporization of saturated methanol) and the energy to decompose the reacting methanol:

$$Q_{tot} = Q_b + Q_{rxn} \tag{35}$$

where Q_b, the energy per unit length to maintain the vapor film, is expressed as

$$Q_b = -2k_v \int_0^{\phi=180} \left(\frac{\partial T}{\partial y}\right)_{y=0} \frac{d}{2}\, d\phi$$

$$= k_v \Delta T_{sat} d \lim_{\phi \to 180^\circ} \int_0^{\phi} \frac{1}{\delta}\, d\phi \approx 2.720 \frac{d\Delta T_{sat} k_v}{\sqrt{2}\, B^{1/4}} \quad (36)$$

The right-hand side of Eq. 36 is obtained by substituting Eqs. 12–14 into Eq. 33 and numerically integrating the result.

Regarding Q_{rxn}, because each mole of methanol reacted yields 2 moles of hydrogen according to Eq. 1 we can evaluate Q_{rxn} by multiplying the enthalpy of reaction with the molar throughput of hydrogen, N_{H_2} from Eqs. 20 and 23, and dividing by 2:

$$Q_{rxn} = \frac{1}{2} \Delta H_R N_{H_2} \quad (37)$$

The enthalpy of reaction, ΔH_R for Eq. 37 is expressed as

$$\Delta H_R = (2h_{f,H_2} + h_{f,CO}) - h_{f,CH_3OH} \quad (38)$$

where the temperature-dependent $h_{f,i}$ values are computed from

$$h_{f,i}(T_2) - h_{f,i}(T_1) = \int_{T_1}^{T_2} c_{p,i} dT + \sum_{\text{transitions}} \Delta_t h_i \quad (39)$$

There are no transitions at the wall, so the rightmost term is zero. Thus, $h_{f,i}$ can be computed for any temperature, provided one knows an expression for $c_{p,i}(T)$ and $h^{\circ}_{f,i}$. Values of standard heats of formation are readily available in tables,[27,28] and a specific heat correlation with temperature for the three components of interest are given in Reid.[23] The result of this integration is

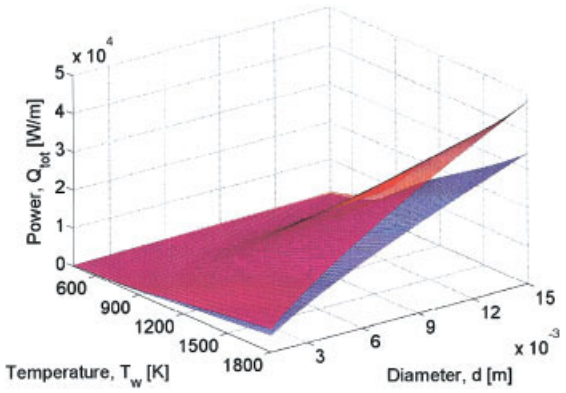

Figure 10. Total power (Q_{tot}) required for methanol decomposition as a function of temperature and diameter.

[Color figure can be viewed in the online issue, which is available at www.interscience.wiley.com.]

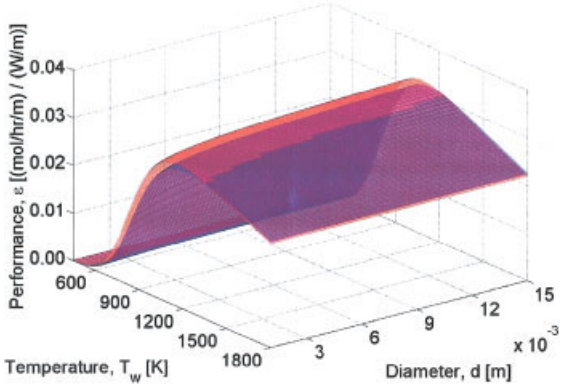

Figure 11. Performance factor as a function of process variables.

[Color figure can be viewed in the online issue, which is available at www.interscience.wiley.com.]

$$\Delta H_R = 73.3 \times 10^3 + 65.7 \times T_w - 5.05 \times 10^{-2} T_w^2 + 3.00 \times 10^{-5} T_w^3 \quad (\text{J/mol}_{\text{meth}}) \quad (40)$$

Because the reaction occurs on the surface of the tube, it is logical to use the wall temperature instead of the average film temperature when computing the heat of reaction. The variation of Q_{tot} with wall temperature and tube diameter is shown in Figure 10. The influence of parameters is comparatively weak up to about 900 K, and then Q_{tot} increases at a higher rate in an almost linear fashion.

Figure 11 combines the variations of hydrogen yield and total power (that is, from Figures 7 and 10, respectively) to show the variation of ε with d and T_w. The trends indicate that, at constant temperature, the variation of ε with tube diameter is comparatively weak. Although increasing d does increase ε and produces a slightly more efficient conversion process, other factors such as economic and size constraints on a FIBOR will limit the largest tube diameter in an application. On the other hand, for a constant tube diameter, ε has a strong dependency on T_w and exhibits an "optimal " operating condition in the sense of a peak of ε. This trend is further illustrated in Figures 12a and 12b, where predictions for a no slip (12a) and zero (12b) shear condition are given (there is little difference between the choice of these two boundary conditions). Figure 12 further shows that the peak value of performance factor has a comparatively small dependency on tube diameter. For 1.5 mm $< d <$ 1.5 cm, the optimal wall temperature is in the range 1080–1225 K. The peak in ε may be explained as follows.

At low temperatures, Q_{tot} is also low (Figure 10) but the hydrogen yield is lower than Q_{tot} for the same tube diameter and wall temperature. The performance factor is accordingly low. As temperature is increased, hydrogen conversion increases faster than Q_{tot} so that ε increases as well. Eventually, hydrogen production tails off as T_w increases as shown in Figure 5 (for a particular tube diameter for illustration) and Figure 7, whereas Q_{tot} continues to increase almost linearly (constrained by the burnout limitation for the tube material) as shown in Figure 10, thus lowering ε at high T_w.

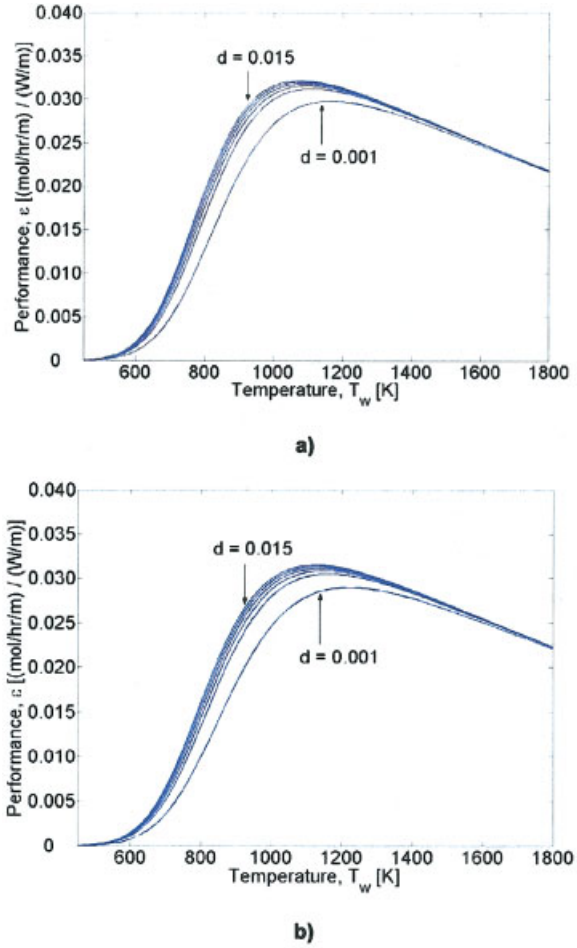

Figure 12. Performance factor as a function of wall temperature for constant tube diameter.

(a) $m = 1$; (b) $m = 2$. [Color figure can be viewed in the online issue, which is available at www.interscience.wiley.com.]

Summary and Conclusions

A platform for catalytic conversion of organic liquids has been analyzed based on film boiling. It is shown that the physical conditions are close to those found in short contact time reactors. The aspects of this new reactor platform are its simplicity, scalability, and as a tool for developing a better understanding of the mechanism of catalytic conversions under real process conditions.

The results indicate that catalytic conversion of methanol on the FIBOR surface produces appreciable amounts of hydrogen gas that suggest its use as a means of hydrogen production. A performance parameter (ε) is used to compare the hydrogen yield with the total energy input to the tube to maintain the vapor film and drive the reaction. This factor has a weak dependency on tube diameter. For methanol using reaction rate values appropriate for a platinum black catalyst, optimal temperatures are predicted to be in the range of 1080 and 1225 K for 1.5 mm $< d <$ 1.5 cm.

Acknowledgments

The authors gratefully acknowledge support of this work by the National Science Foundation through Grant CTS-0500015 with Dr. Alfonso Ortega as the Program Director. Discussions with Mr. Jonah Allaben are also appreciated.

Notation

A = frequency factor of catalyst, mol/(m^2 s^{-1} MPa^{-1})
c_p = specific heat, J kg^{-1} K^{-1}
D = diffusion coefficient, m^2/s
d = tube diameter, m
E = activation energy of catalyst, J/mol
g = gravitational acceleration, m/s^2
$h_{f,i}$ = heat of formation of species i.
ΔH_R = heat of reaction, J/mol
k = thermal conductivity, W m^{-1} K^{-1}
L = latent heat, J/kg
M^* = mass throughput of component, kg h^{-1} m^{-1}
$\bar{n}$ = unit vector
N = molar throughput of component, mol h^{-1} m^{-1}
P = system pressure, MPa
Q = power, W/m
R_o = universal gas constant, J mol^{-1} K^{-1}
T = temperature, K
T_m = minimum film boiling temperature
ΔT_{sat} = wall superheat ($T_w - T_{sat}$), K
u = vapor velocity in the ϕ direction in the vapor film, m/s
v = vapor velocity in the y direction in the vapor film, m/s
W = molecular weight, kg/kmol
w_i = surface rate of reaction of species i, Eq. 4a, kg m^{-2} s^{-1}
Y = mass fraction, dimensionless
y = coordinate normal to heat transfer surface, m

Greek letters

δ = vapor film thickness, m
ε = performance factor, (mol h^{-1} m^{-1})/(W/m)
ϕ = angle from lower stagnation point of cylinder, rad, °
λ = wavelength, m
μ = static viscosity, Pa·s
ρ = density, kg/m^3
σ = surface tension, kg/s^2
ν_i = number of moles of component i produced by the reaction per mole of methanol
χ = arc length around tube circumference (Rϕ)
ϖ_i = reaction rate parameter of species i, Eq. 4b

Subscripts

b = boiling
i = species i (H_2, CO, CH_3OH)
l = liquid
rep = representative value
sat = saturation condition vapor
v = vapor
w = wall

Literature Cited

1. Higgins HM. *A Study of the Reaction of Metals and Water*. AECD-3664. Richland, WA: Hanford Atomic Products Operation; 1955.
2. Ruebsamen WC, Shon FJ, Chrisney JB. *Chemical Reaction between Water and Rapidly Heated Metals*. Report NAA-SR-197. Los Angeles, CA: North American Aviation; October 1952.
3. Crooks RC, Hershall PG, Sorgenti HA, Lemmon AW, Filbert RB. *Studies Relating to the Reaction between Zirconium and Water at High Temperatures*. Report BMI-1154. Columbus, OH: Batelle Memorial Institute; May 1962.
4. Baker L, Just LC. *Studies of Metal–Water Reactions at High Temperatures. III. Experimental and Theoretical Studies of the Zirconium–Water Reaction*. 17th Edition. AEC Research and Development Report, TID-4500, ANL-6548. Argonne, IL: Argonne National Laboratory, U.S. Department of Energy; May 1962.
5. Lustman B. *Zirconium–Water Reactions*. Report WAPD-137. Pittsburgh, PA: Bettis Atomic Power Laboratory; December 1955.

6. Epstein M, Leung JC, Hauser GM, Henry RE. Film boiling on a reactive surface. *Int J Heat Mass Transfer.* 1984;27:1365-1378.
7. Koh JCY. Analysis of film boiling on vertical surfaces. *ASME J Heat Transfer.* 1962;84:55-62.
8. Sakurai A, Shiotsu M, Hata K. A general correlation for pool film boiling heat transfer from a horizontal cylinder to subcooled liquid: Part I. A theoretical pool film boiling heat transfer model including radiation contributions and its analytical solution. *J Heat Transfer.* 1990;112:430-440.
9. Sarma PK, Subrahmanyam T, Rao VD, Bergles AE. Turbulent film boiling on a horizontal cylinder. *Int J Heat Mass Transfer.* 2001;44: 207-214.
10. Liu MH, Yang YM, Maa JR. A general correlation for pool film boiling heat transfer from a horizontal cylinder to saturated binary liquid mixtures. *Int J Heat Mass Transfer.* 1998;41:2321-2334.
11. Okuyama K, Iida Y. Film-boiling heat transfer with a catalytic decomposition reaction. *JSME Int J.* 1994;B37:123-131.
12. Rozovskii AY, Lin GI. Fundamentals of methanol synthesis and decomposition. *Topics Catal.* 2003;42:137-150.
13. Matsumara Y, Tode N. The film boiling reactor: a new environment for chemical processing. *Phys Chem Chem Phys.* 2001;3:1284.
14. Lienhard JH. *A Heat Transfer Textbook*. 2nd Edition. Englewood Cliffs, NJ: Prentice-Hall; 1987:411-417;437-439.
15. Avedisian CT. Bubble growth in superheated liquid droplets. In: *Encyclopedia of Fluid Mechanics*. Houston, TX: Gulf Publishing; 1986:131-153.
16. Avedisian CT, Sullivan JR. A generalized corresponding states method for predicting the limits of superheat of mixtures: Application to the normal alcohols. *Chem Eng Sci.* 1984;39:1033-1042.
17. Lienhard JH, Karimi A. Homogeneous nucleation and the spinodal line. *ASME J Heat Transfer.* 1981;103:61-64.
18. Ohtake H, Koizumi Y. Study on propagative collapse of a vapor film in film boiling (mechanism of vapor-film collapse at wall temperature above the thermodynamic limit of liquid superheat). *Int J Heat Mass Transfer.* 2004;47:1965-1977.
19. Sinha J, Hochreiter LE, Cheung FB. Effects of surface roughness, oxidation level, and liquid subcooling on the minimum film boiling temperature. *Exp Heat Transfer.* 2003;16:45-60.
20. Jordan DP. Film and transition boiling. In: Irvine TF, Hartnett JP, eds. *Advances in Heat Transfer*. Vol. 5. New York, NY: Academic Press; 1968:55-125.
21. Kaviani M. *Principles of Convection*. New York, NY: Springer-Verlag; 1994:587.
22. Bromley LR. Heat transfer in stable film boiling. *Chem Eng Prog.* 1950;46:221-227.
23. Reid RC. *The Properties of Gases and Liquids*. 3rd Edition. New York, NY: McGraw-Hill; 1977.
24. Vargaftik NB. *Handbook of Physical Properties of Liquids and Gases, Pure Substances and Mixtures*. 2nd Edition. New York, NY: Hemisphere Publishing; 1975:404-406.
25. Trimm DL, Onsan ZH. Onboard fuel conversion for hydrogen-fuel-cell-driven vehicles. *Catal Rev.* 2001;43:31-84.
26. Deluga GA, Salge JR, Schmidt LD. Renewable hydrogen from ethanol by autothermal reforming. *Science.* 2004;303:993-997.
27. Beaton CF, Urban BJ, Avedisian CT, Trang W. Physical properties. In: Schlunder E, Beaton C, et al., eds. *Heat Exchanger Design Handbook*. New York, NY: Hemisphere Publishing; 1988.
28. Yaws CL. *Physical Properties: A Guide to the Physical, Thermodynamic and Transport Property Data of Industrially Important Chemical Compounds*. New York, NY: McGraw-Hill; 1977.
29. Williams FW. *Combustion Theory*. Reading, MA: Addison–Wesley; 1965:4,11,15.

Appendix A

The choice of a third-order polynomial for the mass fractions requires four boundary conditions, which are given in Eq. 8. The boundary conditions for Y_i at the solid/vapor interface ($y = 0$) and the vapor/liquid interface ($y = \delta$) are derived from the general species transport equation written for the bulk of a gas in vector form as[29]

$$\nabla \cdot (\rho_v \bar{v} Y_i - \rho_v D_{i,m} \nabla Y_i) = w'''_i \tag{A1}$$

where w'''_i is the volumetric rate of production of species i by chemical reaction in the bulk (kg m^{-3} s^{-1}). By applying Eq. A1 to CO and H_2 (that is, i = CO or H_2 in Eq. A1), the mass fraction of methanol is obtained from Eq. 17. In writing Eq. A1, it has been assumed that the binary diffusion coefficients of all pairs of species are equal. This may not be the case, but nonetheless we assume it even though we use the subscript i,m in Eq. A1 for the diffusion coefficient. For a gas with no chemical reaction in the bulk $w'''_i = 0$ in Eq. A1.

In Eq. A1, $\bar{v}$ is the mass-weighted average velocity vector of the vapor, defined as[29] $\bar{v} = \sum_j Y_j \bar{v}_j$, where $\bar{v}_j$ is the average velocity of molecules of type j (that is, j = CO, CH_3OH, and H_2). It is the ordinary flow velocity of fluid mechanics. The average velocity of molecules of type j, $\bar{v}_j$, is a more complex quantity that requires determination of the velocity distribution function for molecules of species j. The scalar velocity normal to the surface is defined as $v = \bar{v} \cdot \bar{n}$, where $\bar{n}$ is the unit outward normal to either the tube surface or the liquid/vapor interface. $\bar{u}$ would similarly designate the mass-weighted average velocity vector in the ϕ direction (or along the circumference of the tube). However, $\bar{u}$ is not needed in the development of boundary conditions.

For an impermeable wall in which there is no accumulation of mass, a no-slip condition is valid ($v = 0$) regardless of whether a chemical reaction is occurring at the wall. This requirement does not necessarily mean that the individual molecular velocity vectors $\bar{v}_j$ are identically zero at a wall. Rather, it means that the summation, $\sum_j Y_j \bar{v}_j$, must be such that the individual $\bar{v}_j$ have directions that are opposite to the extent that they sum to zero when multiplied by the mass fractions. We also note that the molar-weighted average velocity, $\bar{\bar{v}} \equiv \sum_j n_j \bar{v}_j$, where n_j is the mole fraction of component j, may not in general be zero at a wall where surface reactions occur even if the wall is impermeable. Nonetheless, this issue is not relevant in our analysis because we are always considering the mass-weighted average velocity in the species transport equation.

The condition that the concentrations assume their wall values,

$$Y_i(y = 0) = Y_{i,w} \tag{A2}$$

needs no discussion. The $Y_{i,w}$ are unknown and must be determined as part of the problem.

Additional boundary conditions are obtained by integrating Eq. A1 over the volume (retaining w'''_i in this term-by-term integration) and passing to the limit in which the volume of integration approaches a surface (see Williams[29] for a discussion on this point). The result of this integration and limit process is a boundary condition written in vector form as

$$\left[\rho_v Y_i \left(\bar{v} - D_{i,m} \frac{1}{Y_i} \nabla Y_i \right) \cdot \bar{n} \right] \Bigg|_{y=0 \text{ or } \delta} = w_i|_{y=0 \text{ or } \delta} \tag{A3}$$

where in this limit process w'''_i in Eq. A1 is transformed to a surface rate of reaction of species i, w_i (kg m^{-2} s^{-1}) as given by Eq. 4a. In the coordinates of Figure 1 and with Eq. 4a, Eq. A3 becomes

$$\left.\frac{\partial Y_i}{\partial y}\right|_{y=0 \text{ or } \delta} - \left.\frac{v}{D_{i,m}} Y_i\right|_{y=0 \text{ or } \delta} = -\frac{\varpi_i}{\rho_v D_{i,m}} Y_{i,w} \qquad \text{(A4)}$$

where v is the velocity perpendicular to the interface (solid/gas or liquid/gas) and the coordinate y is measured perpendicular to the boundary (see Figure 1b).

With $v = 0$ at $y = 0$, Eq. A4 reduces to

$$\left.\frac{\partial Y_i}{\partial y}\right|_{y=0} = -\frac{\varpi_i}{\rho_v D_{i,m}} Y_{i,w} \qquad \text{(A5)}$$

This is our second condition for Y_i (Eq. 8a).

For a third condition on Y_i, we return to Eq. A1 written for the "bulk " of the gas in the vapor film. Because there is no chemical reaction in the bulk of the film ($w'''_i = 0$) and we neglect compressibility effects so that $\nabla \cdot (\rho_v \bar{v}) = 0$, Eq. A1 becomes

$$\rho_v \bar{v} \cdot \nabla Y_i - \rho_v D_{i,m} \nabla^2 Y_i = 0 \qquad \text{(A6)}$$

Another condition for Y_i at $y = 0$ is developed from Eq. A6 as follows. We imagine approaching the reactive surface of the tube wall as a limit process. As the tube wall is approached the velocity must gradually vanish. We take this as a limit process:

$$\lim_{y\to 0}(\rho_v \bar{v} \cdot \nabla Y_i - \rho_v D_{i,m} \nabla^2 Y_i) = \lim_{y\to 0}(\rho_v \bar{v} \cdot \nabla Y_i) - \lim_{y\to 0}(\rho_v D_{i,m} \nabla^2 Y_i) = 0 \qquad \text{(A7)}$$

which for the coordinate system of Figure 1 becomes

$$\lim_{y\to 0}\left(\rho_v v \frac{\partial Y_i}{\partial y}\right) - \lim_{y\to 0}\left(\rho_v D_{i,m} \frac{\partial^2 Y_i}{\partial y^2}\right) = 0 \qquad \text{(A8)}$$

Equation A8 shows that diffusion must track with convection. As the wall is approached ($y \to 0$), $v \to 0$. At the same time, Eq. A5 shows that the gradient in mass fraction does not exhibit a singularity. As a result, Eq. A8 reduces to

$$\lim_{y\to 0}\left(\frac{\partial^2 Y_i}{\partial y^2}\right) = \left.\frac{\partial^2 Y_i}{\partial y^2}\right|_{y=0} = 0 \qquad \text{(A9)}$$

which is the third condition on Y_i (Eq. 8a).

A fourth condition, Eq. 8b, is developed at the liquid/vapor interface by applying Eq. A4 at $y = \delta$ where $w_i = 0$:

$$\left.\frac{\partial Y_i}{\partial y}\right|_{y=\delta} - \left.\frac{v}{D_{i,m}} Y_i\right|_{y=\delta} = 0 \qquad \text{(A10)}$$

We assume that CO and H_2 are insoluble in methanol ($Y_{l,\mathrm{CO}} = Y_{l,\mathrm{H_2}} = 0$). Given that a mass balance across the liquid/vapor interface is $v = v_l \rho_l / \rho_v$ then if $v_l = 0$ (stagnant liquid assumption) we conclude that $v = 0$ in Eq. A10 as well, so that

$$\left.\frac{\partial Y_i}{\partial y}\right|_{y=\delta} = 0 \qquad \text{(A11)}$$

where i = CO or H_2.

Taking $v = 0$ at $y = \delta$ (which follows from assuming the liquid to be stagnant) is at odds with the fact that methanol evaporates at the liquid/vapor interface. Nonetheless, there is some historical basis for making this assumption in film boiling analyses: the early analysis of Bromley[22] assumed that the liquid was "stagnant"; Sakurai et al.[8] later compared full numerical solutions for the nonreacting case in which liquid motion was both included and ignored and found that for saturated liquids the predictions are consistent with experimental trends and differ between the two cases by a relatively small numerical factor; and Liu et al.[10] examined mixture transport for the nonreacting case and compared results with the stagnant liquid case with the analysis in which motion in the liquid was considered. Lienhard[14] also noted that in film boiling the liquid is not easily set in motion by flow in the vapor film. More recently, Sarma et al.[9] analyzed the problem of film boiling of a saturated liquid including the effect of turbulence in the vapor film surrounding the cylinder and assumed that the shear at the gas/liquid interface was the same as that at the solid/gas interface, in effect taking the liquid/vapor interface as a rigid boundary. Their results correlated well with their selected data set. All of these approximations are various ways to justify neglecting motion and transport in the liquid.

Appendix B

The integral energy balance of Eq. 10 begins with the first law statement written in a form that neglects kinetic energy:

$$\int_A \rho h \bar{v} \cdot \bar{n} dA = -\int_A \bar{q}'' \cdot \bar{n} dA \qquad \text{(B1)}$$

where the integrations are taken over the surface of a volume (per unit length of the element). For the present discussion this volume is illustrated in Figure B1.

Note that it is bounded on one side by the catalyst-coated tube of radius R, the liquid/vapor interface on another, and the remaining sides by rays at ϕ and $\phi + \Delta\phi$ intersected by arcs of radius $R + \delta$ at ϕ and $R + \delta + \Delta\delta$ at $\phi + \Delta\phi$, as illustrated in Figure B1. Assuming that the liquid is saturated and an equilibrium evaporation process is in effect, Eq. B1 applied to this volume is

$$\left.\int_0^{\delta+\Delta\delta} \rho_v h_v u d y\right|_{\phi+\Delta\phi} - \left.\int_0^{\delta} \rho_v h_v u d y\right|_{\phi} - h_{ls} \rho_l v_l R \Delta\phi = -k \left.\frac{\partial T}{\partial y}\right|_{y=0} R \Delta\phi \qquad \text{(B2)}$$

where h_{Ls} is the enthalpy of saturated liquid. Dividing by $\Delta\phi$ and taking the limit as $\Delta\phi \to 0$, wherein also $\Delta\delta \to 0$, transforms Eq. B2 to

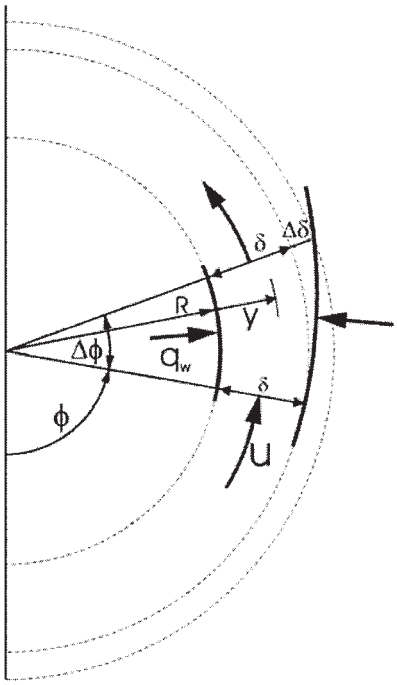

Figure B1. Control volume.

$$\frac{d}{d\phi}\left(\int_0^{\delta}\rho_v h_v u\,dy\right) - h_{ls}\rho_l v_l R = -k\left.\frac{\partial T}{\partial y}\right|_{y=0} R \qquad \text{(B3)}$$

An integral mass balance on the control volume of Figure B1 gives

$$\frac{d}{d\phi}\left(\int_0^{\delta}\rho_v u\,dy\right) = \rho_l v_l R \qquad \text{(B4)}$$

whereupon by combining Eqs. B3 and B4 and grouping terms we get

$$\frac{d}{d\phi}\left[\int_0^{\delta}\rho_v(h_v - h_{ls})u\,dy\right] = -k_v\left.\frac{\partial T}{\partial y}\right|_{y=0} R \qquad \text{(B5)}$$

From the definition of specific heat,

$$c_{pv} = \left.\frac{\partial h_v}{\partial T}\right|_P \qquad \text{(B6)}$$

Assuming that c_{pv} is constant over the temperature range T and the saturated state signified by T_{sat} and h_{vs}, integrating Eq. B6 between T and T_{sat} gives

$$h_v = h_{vs} + c_{pv}(T - T_{sat}) \qquad \text{(B7)}$$

Combining Eqs. B5 and B7, noting that $h_{vs} - h_{ls} \equiv L$ is the heat of vaporization and that $R = d/2$, we obtain

$$\frac{d}{d\phi}\left\{\int_0^{\delta}\rho_v u[L + c_{pv}(T - T_{sat})]dy\right\} = -k_v\frac{d}{2}\left.\frac{\partial T}{\partial y}\right|_{y=0} \qquad \text{(B8)}$$

Integrating Eq. B8 from $\phi = 0$ to ϕ and noting that $u = 0$ at $\phi = 0$ (Eq. 11) gives

$$\rho_v\int_0^{\delta}u[L + c_{pv}(T - T_{sat})]dy = -k_v\frac{d}{2}\int_0^{\phi}\left.\frac{\partial T}{\partial y}\right|_{y=0} d\phi$$

which is Eq. 10.

Manuscript received Apr. 19, 2005, and revision received Jan. 17, 2006.